High Pressure Research

An International Journal

ISSN: 0895-7959 (Print) 1477-2299 (Online) Journal homepage: http://www.tandfonline.com/loi/ghpr20

Pressure-induced disordering and phase transformations in $Eu_2Zr_2O_7$ pyrochlore

Hui Li, Nana Li, Yan Li, Qiang Tao, Yongsheng Zhao, Hongyu Zhu, Yanming Ma, Pinwen Zhu & Xin Wang

To cite this article: Hui Li, Nana Li, Yan Li, Qiang Tao, Yongsheng Zhao, Hongyu Zhu, Yanming Ma, Pinwen Zhu & Xin Wang (2017) Pressure-induced disordering and phase transformations in $Eu_2Zr_2O_7$ pyrochlore, High Pressure Research, 37:2, 256-266, DOI: 10.1080/08957959.2017.1300886

To link to this article: http://dx.doi.org/10.1080/08957959.2017.1300886

HIGH PRESSURE RESEARCH, 2017
VOL. 37, NO. 2, 256–266
http://dx.doi.org/10.1080/08957959.2017.1300886

Taylor & Francis
Taylor & Francis Group

Pressure-induced disordering and phase transformations in $Eu_2Zr_2O_7$ pyrochlore

HPSTAR
417-2017

Hui Li[a,b], Nana Li[c], Yan Li[d], Qiang Tao[a], Yongsheng Zhao[a], Hongyu Zhu[a], Yanming Ma[a], Pinwen Zhu[a] and Xin Wang[a]

[a]State Key Laboratory of Superhard Materials, Jilin University, Changchun, People's Republic of China; [b]College of Science, Guangxi University for Nationalities, Nanning, People's Republic of China; [c]Center for High Pressure Science and Technology Advanced Research, Shanghai, People's Republic of China; [d]College of Physics, Jilin University, Changchun, People's Republic of China

ABSTRACT

The structural properties of pyrochlore $Eu_2Zr_2O_7$ under high pressure have been studied by using Raman spectroscopy and *in situ* angle-dispersive X-ray diffraction (ADXRD). The results of Raman spectra indicate that $Eu_2Zr_2O_7$ undergoes a reversible structural change around 21.2 GPa. The results of Rietveld refinements from *in situ* ADXRD data indicate that the ordered pyrochlore structure (*Fd-3m*) transforms to the defect-cotunnite structure (*Pnma*) at 26.5 GPa. The phase transition is irreversible and the transformation process is mainly induced by the accumulations of anti-site defects of the cation sublattice and Frenkel defects on the anion sublattice. Besides, the <Zr–O> bonds should play a more important role than the <Eu–O> bonds in the process of the phase transformation.

ARTICLE HISTORY
Received 11 December 2016
Accepted 26 February 2017

KEYWORDS
Pyrochlore; synchrotron radiation; Raman spectroscopy; phase transformations

1. Introduction

In recent years, pyrochlore-type rare-earth zirconates ($Ln_2Zr_2O_7$, Ln = rare earth) have received intense interest for various actual and potential applications [1–10]. These zirconates exhibit high stability, low-thermal conductivity, high-melting point, large thermal expansion coefficient, etc. [11–15]. They are candidates for inert matrix fuels to fission 'minor' actinides [16]. In addition, they are widely used as solid oxide fuel cell electrodes, fluorescence screens, thermal-barrier coatings, oxidation catalysts [6], and refractory ceramics in magnetohydrodynamic power generation [17]. Specifically, phase stability and transformation processes are critical to the development of these materials utilized in these applications.

In general, rare-earth zirconate $Ln_2Zr_2O_7$ is present very close to the structure in two forms (the pyrochlore and defect-fluorite structure). It is widely accepted that the pyrochlore–defect-fluorite phase transition can be chemically controlled by varying the size of the A and B cations. The pyrochlore structure (space group: *Fd-3m*) stability at an atmospheric pressure is limited to the range of $1.46 \le r(Ln^{3+}) / r(Zr^{4+}) \le 1.78$, in which the Ln and

CONTACT Pinwen Zhu ✉ zhupw@jlu.edu.cn State Key Laboratory of Superhard Materials, Jilin University, Changchun 130012, People's Republic of China; Xin Wang ✉ xin_wang@jlu.edu.cn State Key Laboratory of Superhard Materials, Jilin University, Changchun 130012, People's Republic of China

Zr cations occupy 16*d* and 16*c* sites, respectively, and the O has two crystallographically distinct oxygen sites (48*f*, 8*b*). The defect-fluorite structure (space group: *Fm-3m*) can form for $r(Ln^{3+}) / r(Zr^{4+}) < 1.46$, in which the cations and anions are randomly distributed on 4a and 8c positions, respectively, with one-eighth of the anion positions vacant. Among the rare-earth zirconates, the $r(Eu^{3+}) / r(Zr^{4+})$ is 1.48 for pyrochlore $Eu_2Zr_2O_7$, which lies close to the pyrochlore–defect-fluorite stability boundary. Besides, $Eu_2Zr_2O_7$ received considerable attention also because of its high ionic conductivity [18, 19]. For $Ln_2Zr_2O_7$ (Ln = La, Nd, Sm, Eu, Gd, Y, Yb), $Eu_2Zr_2O_7$ has the maximum oxide-ion conductivity which was observed in the vicinity of the crystal phase boundary from F- to P-type in these systems [20]. It can be seen that the oxide-ion conductivity is strongly affected by the crystal phases and cation radius ratio. So, research on changes in the structure of $Eu_2Zr_2O_7$ is necessary to investigate the conduction mechanism. Besides, recent experimental and theoretical studies have reported a phase transformation and amorphization of zirconates at around 15–30 GPa [2,21–26]. For example, the ordered pyrochlore $Gd_2Zr_2O_7$ transformed to a defect-cotunnite structure above 15 GPa [23], similar to the case under irradiation [27]; at pressures above 18 GPa, a similar pressure-induced phase transition occurred for $Sm_2Zr_2O_7$ that was studied by angle-dispersive X-ray diffraction (ADXRD) and Raman scattering methods [21]; the transition pressures were 21 and 22 GPa for $La_2Zr_2O_7$ and $Nd_2Zr_2O_7$, respectively [25,26].

In this paper, pyrochlore $Eu_2Zr_2O_7$ has been successfully synthesized using standard solid state reaction method. The structural changes of $Eu_2Zr_2O_7$ under high pressure have been investigated using Raman spectra and angle-dispersive synchrotron X-ray powder diffraction up to 33.2 GPa at room temperature. A pressure-induced phase transition is observed, and the detailed analysis of the results and transformation mechanism is carried out.

2. Experimental methods

The highly pure oxides of Eu_2O_3 (99.99%, powder) and ZrO_2 (99.95%, powder) were used as the starting materials. The raw materials with nominal compositions of $Eu_2Zr_2O_7$ were uniformly mixed in an agate mortar. The obtained powder was pressed into small pellets and was calcined at 1773K in air for 12 h. The crystal phase structures of the synthesized sample are characterized by a Rigaku D/max-2500 X-ray powder diffraction (XRD) with Cu Kα radiation ($\lambda = 1.54056$ Å) in the range 2θ from 10° to 90° at a scanning rate of 4°/min.

A diamond anvil cell (DAC) was utilized to generate high pressure with the T301 stainless steel as the gasket, which was preindented to a 50 µm thickness. The powder samples were loaded into the DAC along with chips of ruby for measuring the sample pressure [28]. Silicone oil was chosen as the pressure medium to provide hydrostatic conditions in Raman spectroscopy measurements, and 16:3:1 methanol/ethanol/water mixture was chosen for *in situ* ADXRD measurements. High pressure Raman spectra were collected with Renishaw InVia spectrometer using a 532 nm He–Ne laser and a 50 times Leica optical microscope. *In situ* ADXRD experimental runs were conducted at BLX17C of National Synchrotron Light Source at Brookhaven, using the angle-dispersive XRD mode ($\lambda = 0.4049$ Å). The experimental parameters, including the distance between sample and detector, were calibrated using the CeO_2 standard materials. The FIT2D software was employed to convert the image plate records into intensity versus diffraction angle

2θ patterns. Rietveld analyses were performed with the software GSAS [29]. The refined parameters were the lattice constants, the atomic position of oxygen, a Chebyshev polynomial background, Pseudo-Voigt profile parameters, a common isotropic thermal parameter for all atom sites, and an overall intensity scaling factor.

3. Results and discussion

3.1. X-ray diffraction patterns at ambient pressure

The crystal structure of $Eu_2Zr_2O_7$ is consistent with the earlier report to have the *Fd-3m* symmetry [30], i.e. it has a pyrochlore structure characterized by X-ray powder diffraction and Rietveld refinement of the resulting diffraction pattern. The refined patterns of $Eu_2Zr_2O_7$ together with the calculated profile and their differences and the merits of the refinement are presented in Figure 1. The merit of the refinement is $R_p = 7.91\%$, $R_{wp} = 6.18\%$ at ambient pressure. The lattice parameter is $a = 10.5518(9)$ Å and $Z = 8$. The refined atomic position coordinates are given in Table 1. Currently, standard practice is to formulate oxide pyrochlores as $A_2B_2O_6O'$ and to place the B ion at 16*c*, A at 16*d*, O at 48*f*, and O′ at 8*b*. The A-site (16*d*) coordination polyhedron is a distorted cube that generally contains larger cations; the B-site (16*c*) is a distorted octahedron. It is worth noting that there is only one adjustable positional parameter x for the O atom in 48*f*. The schematic diagrams of the pyrochlore structure (P-type) are presented in the inset of Figure 1.

3.2. Raman spectra at high pressures

According to the factor group analysis based on the *Fd-3m*, the structure of $Eu_2Zr_2O_7$ yields the irreducible representation at the Brillouin zone center as follows:

$$G = A_{1g} + E_g + 2F_{1g} + 4F_{2g} + 3A_{2m} + 3E_m + 8F_{1m} + 4F_{2m} \tag{1}$$

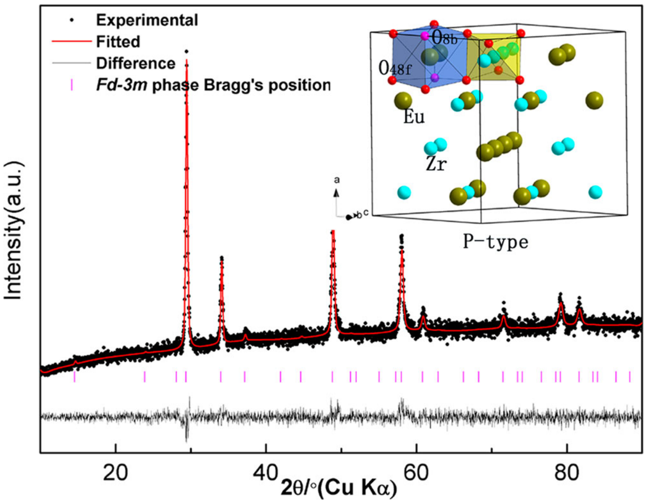

Figure 1. Observed (solid circles) and calculated (solid lines) diffraction patterns of $Eu_2Zr_2O_7$ at ambient pressure. The difference curve and the tick marks for the calculated reflection positions are plotted at the bottom. The upper right inset shows polyhedral views of $Eu_2Zr_2O_7$ in P-type phase.

Table 1. The refined atomic coordinates of the ambient pressure cubic phase and the high pressure orthorhombic phase of $Eu_2Zr_2O_7$ at 33.2 GPa.

Compounds	$Eu_2Zr_2O_7$ (at ambient pressure)	$Eu_2Zr_2O_7$ (33.2 GPa)
Crystal system	Cubic	Orthorhombic
Space group	*Fd-3m*(227)	*Pnma*(62)
a/Å	10.5518 (9)	5.384 (11)
b/Å	10.5518 (9)	3.247 (4)
c/Å	10.5518 (9)	6.470 (9)
Atoms	Wyckoff (*x y z*)	Wyckoff (*x y z*)
Eu	16*d* (0.5 0.5 0.5)	4*c* (0.2470(6) 0.2500 0.3717(15))
Zr	16*c* (0 0 0)	4*c* (0.2470(6) 0.2500 0.3717(15))
O(1)	48*f* (0.125 0.125 0. 0.3496(8))	4*c* (0.0284(4) 0.2500 0.6785(7))
O(2)	8*b* (0.325 0.325 0.325)	4*c* (0.1444(3) 0.2500 0.0721(10))
Residuals[a] / %	R_{wp}: 7.91% R_p: 6.18%	R_{wp}: 4.74% R_p: 2.72%

[a] R_{wp} and R_p as defined in GSAS [21].

Among these normal modes, only A_{1g}, E_g, $4F_{2g}$ are Raman active and $8F_{1\mu}$ are infrared active. Others are inactive modes. Figure 2 shows the selected Raman spectra of $Eu_2Zr_2O_7$ under high pressure at room temperature. From Figure 2, it can be seen that Raman spectra show the major Raman modes of the pyrochlore-type structure such as E_g at 303 cm^{-1}, A_{1g} at 541 cm^{-1}, one F_{2g} at 390 cm^{-1}, and another F_{2g} at 585 cm^{-1}, which are assigned to the O–Eu–O bending, Eu–O stretch, Zr–O stretch, and Eu–O stretch modes, respectively, which was also observed in the previous analysis [31]. Other F_{2g} modes are too weak to be observed.

The frequency shifts of all the observed Raman modes with pressure are shown in Figure 3. With increasing pressures, all the Raman bands are shifted to the higher frequencies up to 18.9 GPa. Dramatic spectral changes occur at 21.2 GPa, as two new peaks appear, which are marked by green lines in Figure 2. These two Raman modes are

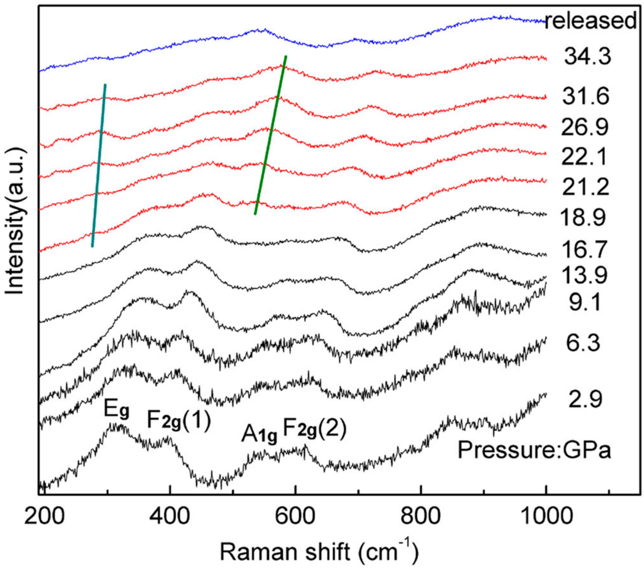

Figure 2. Selected Raman spectra of $Eu_2Zr_2O_7$ under high pressure. Two new peaks that appeared above 21.2 GPa are marked with green lines.

located at 266 and 541 cm^{-1}, which clearly identified a pressure-induced phase transition at 21.2 GPa. The spectrum of $Eu_2Zr_2O_7$, as it has recovered from 34.3 GPa, shows a quite different character from the starting pyrochlore, so the pressure-induced structure transition in $Eu_2Zr_2O_7$ is irreversible. In order to further understand the structural changes of $Eu_2Zr_2O_7$, high pressure *in situ* ADXRD was measured.

3.3. In situ *ADXRD measurement at high pressures*

Selected XRD patterns of $Eu_2Zr_2O_7$ up to 33.2 GPa are shown in Figure 4(a). From ambient pressure up to 24.3 GPa, the pattern is that of a typical P-type structure. It also can be seen that all diffraction peaks markedly shift to larger diffraction angles as the pressure increases. At 26.5 GPa, it can be clearly seen that some new peaks are emerging from the original phase, indicating a high pressure phase forms from P-type $Eu_2Zr_2O_7$. From 26.5 GPa to the highest pressure we reached, pyrochlore phase and high pressure phase coexist, which might be explained as the inherent sluggish nature of the transition and the kinetic effects of the transition. Also, the phase transition is irreversible as the diffraction peaks of the HP structure remain after the complete release of pressure. Compared to previous research on other zirconates, the high pressure phase of $Eu_2Zr_2O_7$ may have a structure similar to that of defect-fluorite (F-type) [21,23], where the cations of Eu^{3+} and Zr^{4+} are disordered on the A and B sites. Analyzed by Rietveld refinement using the GSAS software, all the diffraction peaks of the new phase could be explained using an orthorhombic unit cell based on *Pnma* phase (defect-cotunnite structure). Both cations and anions are randomly distributed on 4*c* positions in the defect-cotunnite structure and one-eighth of the anions are missing. In the defect fluorite (F-type) structure, the Eu has an equivalent bonding environment as Zr, and the defect F-type structure is isotropic with the cubic ZrO_2 except for the absence of one-eighth of the anions. There are two other polymorphs [32] for ZrO_2 besides the high-temperature cubic phase: the monoclinic

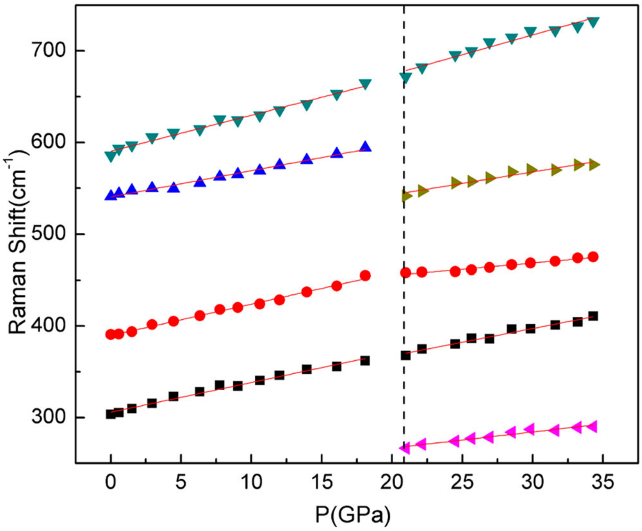

Figure 3. Pressure dependences of Raman shifts of $Eu_2Zr_2O_7$.

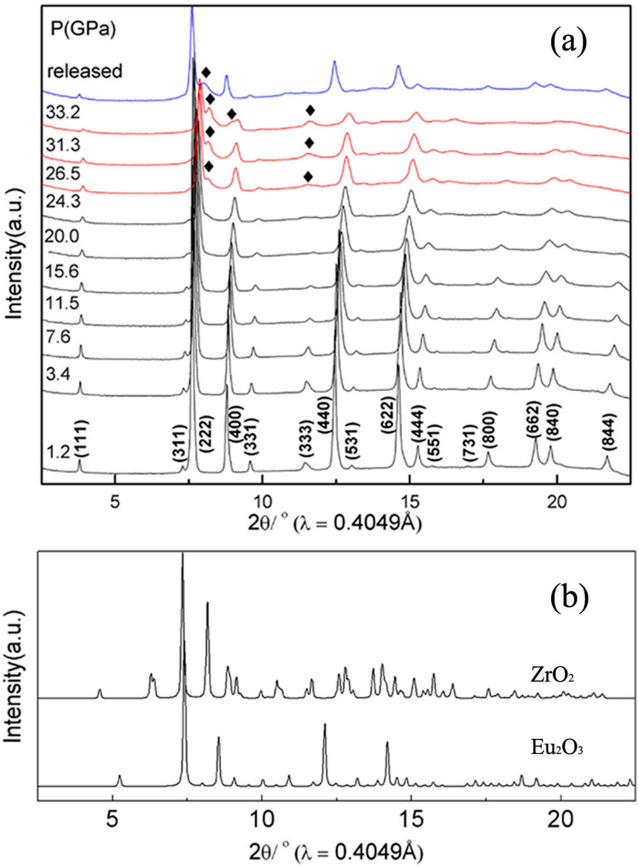

Figure 4. (a) Representative X-ray diffraction patterns of $Eu_2Zr_2O_7$ at various pressures. The pyrochlore structure is stable up to 24.3 GPa and transforms to a defect-cotunnite structure at higher pressures. The top blue pattern was taken from the quenched samples after the release of pressure. The black rhombus represents the diffraction peaks from the high pressure phase. (b) The difference X-ray powder patterns of cubic Eu_2O_3 and monoclinic ZrO_2 at ambient pressure.

phase, stable below 1500 K, and the tetragonal phase, stable between 1500 and 2560 K. Both of these structures can be considered to be distorted fluorite structures. The Eu and Zr cations in the defect-cotunnite structure have an equivalent bonding environment, the defect-cotunnite structure also can be considered to be distorted in the defect-fluorite structure. The fitting result of $Eu_2Zr_2O_7$ at the highest pressure point is shown in Figure 5, where the merit of the refinement is $R_p = 2.72\%$, $R_{wp} = 4.74\%$. The atomic structure of the cotunnite-type (C-type) unit cell is shown in the inset of Figure 5 and the determined structural parameters are listed in Table 1.

Based on the knowledge of the pyrochlore structure, the only variable atomic coordinate x_{48f} can be used for quantifying the degree of disorder of the anion. Figure 6(a) shows the pressure dependence of x_{48f} with pressure. At ambient pressure $x = 0.335$, it increases to 0.348 at 24.3 GPa, thus approaching the ideal defect F-type structure ($x = 0.375$), which is consistent with the analysis of the high pressure phase (a disordered defect-fluorite structure). Cation disorder can be quantified with the cation order

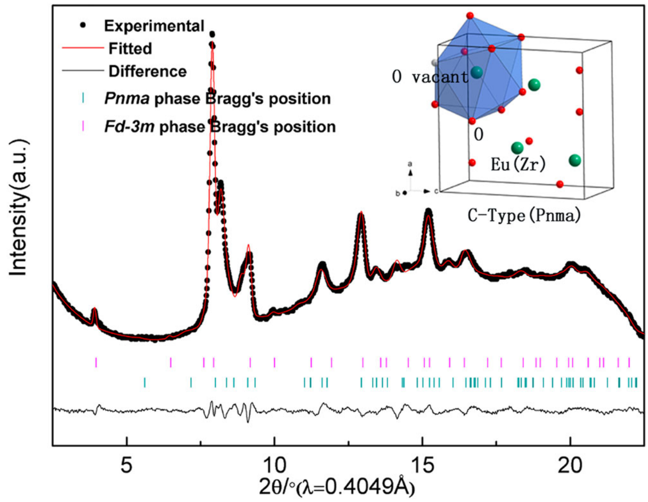

Figure 5. Observed (solid circles) and calculated (solid lines) diffraction patterns of $Eu_2Zr_2O_7$ at 33.2 GPa. The upper right inset shows polyhedral views of $Eu_2Zr_2O_7$ in C-type phase.

parameter Φ_C defined as [33]

$$\Phi_C = 2A_A - 1 \tag{1}$$

where A_A is the actual A ion occupation of the A site. Φ_C is 1 and 0 in ideal pyrochlore and ideal defect-fluorite structures, respectively. Below 24.3 GPa, the observed XRD patterns of $Eu_2Zr_2O_7$ can be well refined with the pyrochlore structure model after accounting for the cationic disordering. Figure 6(b) shows the degree of cation disordering in $Eu_2Zr_2O_7$ at

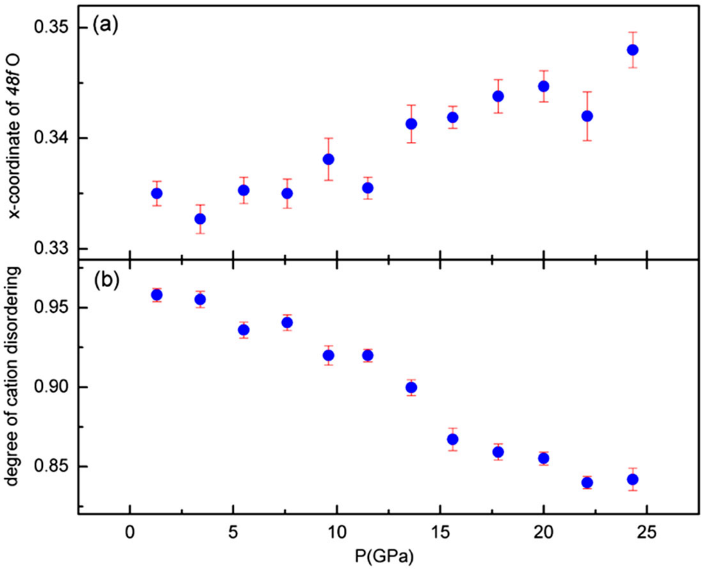

Figure 6. (a) Pressure dependence of x_{48f}; (b) Degree of cation disordering with the increase of pressure.

various pressures. With an increase of pressure, the degree of cation disordering between Eu^{3+} and Zr^{4+} decreases from 0.958 at ambient pressure to 0.842 at a pressure of 24.3 GPa. Thus, we can clearly see that anti-site defects (mixed occupancy by $Eu^{3+}$and Zr^{4+}) of the cation sublattice and Frenkel defects (interstitial and vacancy pairs) on the anion sublattice are created in $Eu_2Zr_2O_7$ pyrochlores by applying pressure. The accumulation of these defects plays a particularly important role in the phase transition process.

At the transition pressure of 26.5 GPa, the average <cation–anion> bond distance (2.366 Å) in the C-type $Eu_2Zr_2O_7$ is nearly the same as the <Eu–O> bond distance (2.347 Å), but much larger than the <Zr–O> bond length (2.044 Å) in the P-type structure, indicating that <Zr–O> bonds should undergo more significant change during the phase transition, as compared with the <Eu–O> bonds. Besides, Figure 7 shows the variation of bond length with pressure for $Eu_2Zr_2O_7$, which indicates that the <Zr–O> bonds are less compressible than <Eu–O> bonds. The decreased compressibility of the <Zr–O> bonds relative to the <Eu–O> bonds signifies <Zr–O> bonds more easily undergo changes upon compression. These results suggest that the <Zr–O> bonds should play a more important role than the <Eu–O> bonds in the P-type → C-type phase transformation.

The pressure dependence of the unit cell volume for the P-type structure and the high pressure phase of $Eu_2Zr_2O_7$ are shown in Figure 8. A large volume drop by approximately 12.0% is observed at the phase transition. The data were fitted with a third-order Birch–Murnaghan equation of state [34]:

$$P = \frac{3.0}{2}B_0\left[\left(\frac{V_0}{V}\right)^{7/3} - \left(\frac{V_0}{V}\right)^{5/3}\right] \times \left(1 + \frac{3.0}{4}(B'_0 - 4) \times \left[\left(\frac{V_0}{V}\right)^{2/3} - 1\right]\right), \qquad (2)$$

where B_0 is the bulk modulus and B'_0 is its pressure derivative at the equilibrium volume V_0. In order to facilitate the comparison of B_0 values, we have followed the standard procedure of setting $B'_0 = 4$. The fitting results for the pyrochlore $Eu_2Zr_2O_7$ give the bulk modulus B_0 = 229(6) GPa.

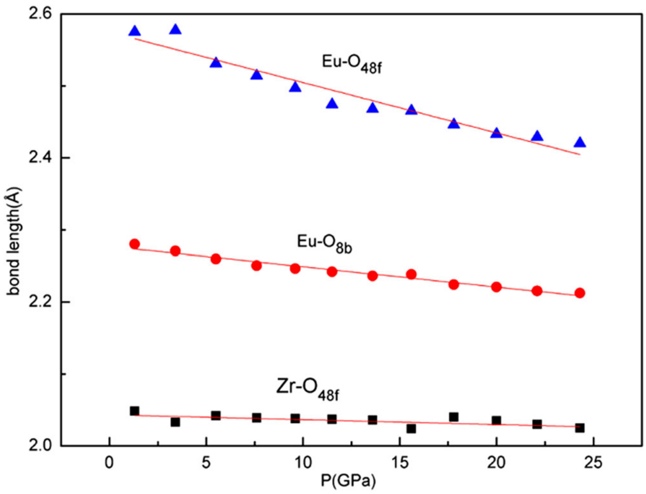

Figure 7. The cation–anion bond lengths in pyrochlore $Eu_2Zr_2O_7$ at various pressures.

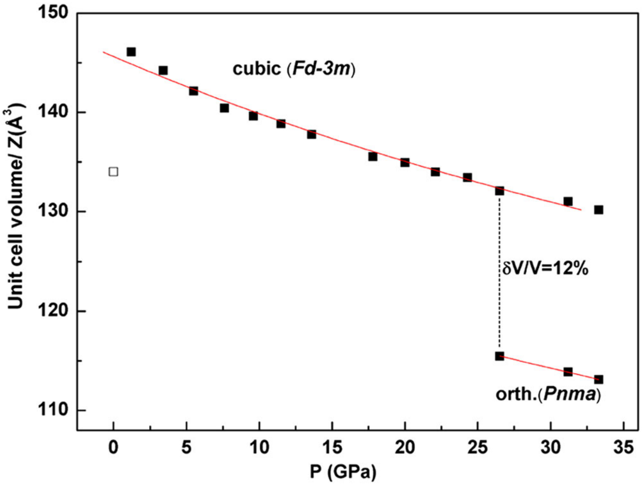

Figure 8. The calculated unit cell volume per formula unit of $Eu_2Zr_2O_7$ at different pressures. The pyrochlore structure shrinks about 12.0% in volume during phase transition to the high pressure phase (defect-cotunnite structure).

4. Conclusions

In summary, the structural behavior of pyrochlore $Eu_2Zr_2O_7$ was studied under high pressure by means of Raman spectroscopy and *in situ* ADXRD, and an irreversible structural phase was obtained under high pressure. We have observed abrupt changes of the Raman spectra around 21.2 GPa. *In situ* ADXRD measurements confirmed the phase transition above 24.3 GPa and revealed the ordered pyrochlore (P-type) transforming to the defect-cotunnite (C-type) structure (a disordered defect-fluorite-type structure). Pressure-induced atomic disordering was observed in pyrochlore $Eu_2Zr_2O_7$. The phase transition process was induced by the accumulations of anti-site defects of the cation sublattice and Frenkel defects on the anion sublattice. Moreover, the variations of average bond lengths with pressure suggested that the <Zr–O> bonds should play a more important role than the <Eu–O> bonds in the P-type → C-type phase transformation.

Acknowledgements

We acknowledge Dr Chen Zhiqiang for technical support with the high pressure experiments at the BLX17C of the NSLS synchrotron.

Disclosure statement

No potential conflict of interest was reported by the authors.

Funding

This work was supported by the National Natural Science Foundation of China under Grant Nos. 51172091, 11304114, and 11534003, and open project of State Key Laboratory of Superhard Materials (Jilin University).

References

[1] Lang M, Zhang FX, Zhang JM, et al. Nanoscale manipulation of the properties of solids at high pressure with relativistic heavy ions. Nat Mater. 2009;8:793–797.

[2] Zhang FX, Wang JW, Lian J, et al. Phase stability and pressure dependence of defect formation in Gd_2 Ti_2O_7 and $Gd_2Zr_2O_7$ pyrochlores. Phys Rev Lett. 2008;100:045503.

[3] Sickafus KE, Minervini L, Grimes RW, et al. Radiation tolerance of complex oxides. Science. 2000;289:748–751.

[4] Crocombette JP, Chartier A, Weber WJ. Atomistic simulation of amorphization thermokinetics in lanthanum pyrozirconate. Appl Phys Lett. 2006;88:051912.

[5] Wang C, Wang Y, Cheng Y, et al. Preparation and thermophysical properties of nano-sized $Ln_2Zr_2O_7$ (Ln = La, Nd, Sm, and Gd) ceramics with pyrochlore structure. J Mater Sci. 2012;47:280–284.

[6] Rabasovic MS, Sevic D, Krizan J, et al. Characterization and luminescent properties of Eu^{3+} doped $Gd_2Zr_2O_7$ nanopowders. J Alloys Compd. 2015;622:292–295.

[7] Lian J, Zu XT, Kutty KVG, et al. Ion-irradiation-induced amorphization of $La_2Zr_2O_7$ pyrochlore. Phys Rev B. 2002;66:054108.

[8] Zhang Y, Weber WJ, Shutthanandan V, et al. Damage evolution on Sm and O sublattices in Au-implanted samarium titanate pyrochlore. J Appl Phys. 2004;95:2866–2872.

[9] Liu ZG, Ouyang JH, Zhou Y. Preparation and thermophysical properties of $(Nd_xGd_{1-x})_2Zr_2O_7$ ceramics. J Mater Sci. 2008;43:3596–3603.

[10] Uno M, Kosuga A, Okui M, et al. Photoelectrochemical study of lanthanide zirconium oxides, $Ln_2Zr_2O_7$ (Ln = La, Ce, Nd and Sm). J Alloys Compd. 2006;420:291–297.

[11] Vassen R, Cao X, Tietz F, et al. Zirconates as new materials for thermal barrier coatings. J Am Ceram Soc. 2000;83:2023–2028.

[12] Liu B, Wang JY, Zhou YC, et al. Theoretical elastic stiffness, structure stability and thermal conductivity of $La_2Zr_2O_7$ pyrochlore. Acta Mater. 2007;55:2949–2957.

[13] Matteucci F, Cruciani G, Dondi M, et al. Crystal structural and optical properties of Cr-doped $Y_2Ti_2O_7$ and $Y_2Sn_2O_7$ pyrochlores. Acta Mater. 2007;55:2229–2238.

[14] Wan CL, Qu ZX, Du AB, et al. Influence of B site substituent Ti on the structure and thermophysical properties of $A_2B_2O_7$-type pyrochlore $Gd_2Zr_2O_7$. Acta Mater. 2009;57:4782–4789.

[15] Yao H, Ouyang L, Ching WY. Ab initio calculation of elastic constants of ceramic crystals. J Am Ceram Soc. 2007;90:3194–3204.

[16] Ewing RC, Weber WJ, Lian J. Nuclear waste disposal – pyrochlore ($A_2B_2O_7$): nuclear waste form for the immobilization of plutonium and ‘minor’ actinides. J Appl Phys. 2004;95:5949–5971.

[17] Chapman RA, Meadowcroft DB, Walkden AJ. Some properties of zirconates and stannates with the pyrochlore structure. J Phys D Appl Phys. 1970;3:307–319.

[18] Shlyakhtina AV, Knotko AV, Boguslavskii MV, et al. Effect of non-stoichiometry and synthesis temperature on the structure and conductivity of $Ln_{2+x}M_{2-x}O_{7-x/2}$ (Ln = Sm–Gd; M = Zr, Hf; x = 0–0.286). Solid State Ionics. 2007;178:59–66.

[19] Shlyakhtina AV, Kolbanev IV, Knotko AV, et al. Ionic conductivity of $Ln_{2+x}Zr_{2-x}O_{7-x/2}$ (Ln = Sm-Gd) solid solutions. Inorg Mater. 2005;41:854–863.

[20] Yamamura H, Nishino H, Kakinuma K, et al. Electrical conductivity anomaly around fluorite–pyrochlore phase boundary. Solid State Ionics. 2003;158:359–365.

[21] Zhang FX, Liana J, Beckera U, et al. Structural distortions and phase transformations in $Sm_2Zr_2O_7$ pyrochlore at high pressures. Chem Phys Lett. 2007;441:216–220.

[22] Zhang FX, Lang M, Becker U, et al. High pressure phase transitions and compressibilities of $Er_2Zr_2O_7$ and $Ho_2Zr_2O_7$. Appl Phys Lett. 2008;92:011909.

[23] Zhang FX, Lian J, Becker U, et al. High-pressure structural changes in the $Gd_2Zr_2O_7$ pyrochlore. Phys Rev B. 2007;76:214104.

[24] Kumar NRS, Shekar NVC, Sahu PC. Pressure induced structural transformation of pyrochlore $Gd_2Zr_2O_7$. Solid State Commun. 2008;147:357–359.

[25] Zhang FX, Lang M, Liu ZX, et al. Pressure-Induced disordering and anomalous lattice expansion in $La_2Zr_2O_7$ pyrochlore. Phys Rev Lett. 2010;105:015503.

[26] Xiao HY, Zhang FX, Gao F, et al. Zirconate pyrochlores under high pressure. Phys Chem Chem Phys. 2010;12:12472.

[27] Wang SX, Begg BD, Wang LM, et al. Radiation stability of gadolinium zirconate: a waste form for plutonium disposition. Mater Res. 1999;14:4470–4473.

[28] Mao HK, Xu J, Bell PM. Calibration of the ruby pressure gauge to 800 kbar under quasi-hydrostatic conditions. J Geophys Res. 1986;91:4673–4676.

[29] Larson AC, Von Dreele RB. General structure analysis system (GSAS). Los Alamos (NM): Los Alamos National Laboratory; 1994. (LAUR 86-748).

[30] Hagiwara T, Yamamura H, Nishino H. Mater Sci Eng. 2011;18:132003.

[31] Xia XL, Liu ZG, Ouyang JH, et al. Preparation, structural characterization, and enhanced electrical conductivity of pyrochlore-type $(Sm_{1-x}Eux)_2Zr_2O_7$ ceramics. Fuel Cells. 2012;12:624–632.

[32] Yashima M, Hirose T, Katano S, et al. Structural changes of ZrO_2-CeO_2 solid solutions around the monoclinic-tetragonal phase boundary. Phys Rev B. 1995;51:8018–8025.

[33] Tuller HL, Moon PK. Fast ion conductors: future trends. Mater Sci Eng B. 1988;1:171–191.

[34] Birch F. Finite strain isotherm and velocities for single-crystal and polycrystalline NaCl at high pressures and 300°K. J Geophys Res. 1978;83:1257–1268.